frontiers | Frontiers in Marine Science

TYPE Original Research
PUBLISHED 08 January 2024
DOI 10.3389/fmars.2023.1302064

OPEN ACCESS

EDITED BY
NicolòColombani,
Marche Polytechnic University, Italy

REVIEWED BY
Luigi Tosi,
National Research Council (CNR), Italy
Gianluigi Busico,
University of Campania Luigi Vanvitelli, Italy

*CORRESPONDENCE
Shenliang Chen
slchen@sklec.ecnu.edu.c
Guangquan Chen
chenguangquan@fio.org.cn

RECEIVED 26 September 2023
ACCEPTED 13 December 2023
PUBLISHED 08 January 2024

CITATION
Cui Z, Chen G, Chen S, Yu H, Chen K, Ran B, Fu T, Lyu W, Wang Y, Jiang X and Zhong X (2024) Groundwater salinization under the influence of paleo sea-level fluctuation: a case study in southern Laizhou Bay, China. *Front. Mar. Sci.* 10:1302064. doi: 10.3389/fmars.2023.1302064

Groundwater salinization under the influence of paleo sea-level fluctuation: a case study in southern Laizhou Bay, China

Zhen Cui[1,2], Guangquan Chen[2*], Shenliang Chen[1*], Hongjun Yu[2], Keke Chen[3], Baichuan Ran[1], Tengfei Fu[2], Wenzhe Lyu[2], Yancheng Wang[2], Xueyan Jiang[4] and Xihuang Zhong[4]

[1]State Key Laboratory of Estuarine and Coastal Research, East China Normal University, Shanghai, China, [2]Key Laboratory of Marine Geology and Metallogeny, First Institute of Oceanography, Ministry of Natural Resources, Qingdao, China, [3]North China Sea Ecological Center, Ministry of Natural Resources, Qingdao, China, [4]Department of Chemistry and Chemical Engineering, Ocean University of China, Qingdao, China

The groundwater environment in low-lying coastal regions is significantly impacted by global sea-level fluctuation. In Laizhou Bay, three large-scale transgressions have occurred since the late Pleistocene, resulting in the transformation of ancient seawater into brine. This brine has become a major contributor to groundwater salinity in the area. This study establishes a correlation between groundwater occurrence and paleoclimate changes in Laizhou Bay using borehole sediment data. The source and mechanism of groundwater salinity are analyzed based on sediment pore water characteristics and hydrogen and oxygen isotopes. The study reveals that the stratigraphic structures in the area consist of four layers: a Holocene transgressive layer, a continental confining bed from the late Pleistocene, a Cangzhou transgressive layer from the late Pleistocene, and a fluvial aquifer from the middle Pleistocene. All aquifers in the study area have been infiltrated by modern seawater, with the uppermost Holocene aquifer influenced by evaporation and leaching processes, the central late Pleistocene aquifer remaining relatively stable, and the lower middle Pleistocene aquifer affected by subsurface low salinity runoff and exhibiting an increasing trend with depth. Given the presence of numerous hydrogeological environments globally that are similar to the study area, the obtained mechanisms of groundwater salinization in this study will provide theoretical support for groundwater management in similar regions worldwide.

KEYWORDS

groundwater salinization mechanisms, porewater analysis, hydrochemical characteristics, stable isotope characteristics, southern coast of Laizhou Bay, global sea level fluctuation

Highlights

- Paleo sea-level changes primarily control the distribution of coastal groundwater.
- Groundwater exploitation and modern seawater intrusion are the main factors influencing salinization mechanisms.
- Modern seawater intrusion basically displaces the paleo-brine.

1 Introduction

Coastal regions at lower elevations worldwide are highly vulnerable to the impacts of climate change, such as rising sea levels, tidal inundation, and storm surges. These factors contribute to the intrusion of seawater into coastal groundwater, leading to salinization. Groundwater salinization has been observed in numerous regions across various countries, including China (Guo and Huang, 2003). This salinization not only degrades groundwater quality but also reduces water resources for industrial, agricultural, and domestic purposes, exacerbating freshwater scarcity (Bordbar et al., 2023; Tomaszkiewicz et al., 2014). Additionally, high salinity levels in groundwater, particularly in arid and semi-arid regions, can increase soil salinity through capillary action, affecting agricultural productivity. Global groundwater salinization has gained significant attention from the international community (Yakirevich et al., 1998; Moussaoui et al., 2023; Parisi et al., 2023). The main mechanisms contributing to groundwater salinization are: (1) Modern seawater intrusion due to rising sea levels caused by global warming (Laattoe et al., 2013; Agossou et al., 2022; Balasubramanian et al., 2022; Sathish et al., 2022); (2) Modern seawater intrusion resulting from excessive groundwater extraction and hydraulic reclamation (Chen et al., 2021;Lio et al., 2015); and (3) Transformation of paleo-seawater preserved in marine strata during transgression into modern brine, which has significantly higher salinity levels and a larger extent of salinization (Sanford et al., 2013; Larsen et al., 2017). Among these mechanisms, brine-induced salinization is the most severe (Giambastiani et al., 2013; Liu et al., 2017; Chen et al., 2021).

Understanding groundwater mixing processes is crucial for sustainable groundwater utilization in coastal regions. Extensive research has been conducted over the past 60 years to better comprehend coastal aquifer flow and transport processes. Electrical resistivity tomography (ERT) is a widely used method in coastal hydrogeology for visualizing subsurface resistivity distribution in 2D or 3D (Werner et al., 2013). It has proven effective in identifying mixing zones between saltwater and freshwater (Acworth & Dasey, 2003). Chemical composition analysis of coastal groundwater has also been utilized to determine the origin of dissolved salts. While seawater intrusion is the primary cause of increased groundwater salinity, other sources and processes can contribute as well. A multi-tracer approach combining hydrochemical and isotope data has been successful in identifying salinity sources (Han et al., 2014; Petelet-Giraud et al., 2016).

The southern coast of Laizhou Bay is one of the most heavily impacted areas by groundwater salinization globally, affecting an extensive land area of over 25,000 km^2. This region has experienced three large-scale transgression events due to global sea level fluctuations caused by glacial-interglacial climate change since the late Pleistocene (Wang et al., 1981; Xu et al., 1997). The trapped paleo-seawater in marine strata has undergone various evolutionary processes, such as evaporation, fractionation, and ion exchange with sediments, resulting in the formation of brine (Gao et al., 2015). Groundwater resources from the southern coast of Laizhou Bay have been utilized for agricultural, industrial, and domestic water needs in North Shandong Province for several decades (Han et al., 2020), leading to intensive groundwater exploitation. The mixing mechanisms of different groundwater types in the region, including seawater with freshwater, seawater with brine, and freshwater with brine, are complex due to overexploitation. Consequently, the sources and mixing mechanisms of groundwater salinization at different depths in the sea-land interaction zone, influenced by paleo sea-level fluctuations since the late Pleistocene, remain a complex and unresolved scientific challenge.

Throughout the Quaternary period, the position of the interface between fresh and saline water has been constantly changing. These fluctuations, which could reach up to 130 m (Chappell et al., 1996), resulted in the emergence or submergence of large coastal areas (Vallejos et al., 2018). Consequently, the presence of ancient seawater trapped in coastal aquifers is common worldwide. This study aims to identify the source and mechanisms of groundwater salinization at different depths in areas where brine is present. Previous research has shown that the profiles of natural tracers in porewaters of clay-rich sediments can serve as reliable records of paleo-hydrogeological changes (Hendry and Woodbury, 2007). By analyzing environmental tracers such as chloride (Cl^-) and bromide (Br^-) in porewater, along with sediment core data on depositional facies associations, the origin of salinity can be determined (Cartwright et al., 2004; Edmunds et al., 2006; Alcalá and Custodio, 2008; Alessandrino et al., 2023; Rajmohan et al., 2021). The source of water can be identified using stable isotopes of hydrogen (δD) and oxygen ($\delta^{18}O$). (Han et al., 2020; Carretero et al., 2022; Dun et al., 2022). In this study, we investigated the hydrochemical characteristics, stable isotopes of hydrogen and oxygen, and sedimentary environmental changes in the study area to understand the origin and mechanisms of groundwater salinization at different depths.

2 Materials and methods

Brine is commonly found in both inland and coastal areas worldwide. In the coastal region, there are several other areas similar to our study area that also have brine in their aquifers. These areas are affected by seawater intrusion, freshwater recharge, and groundwater extraction (Figure 1) (Lenahan & Bristow, 2010;

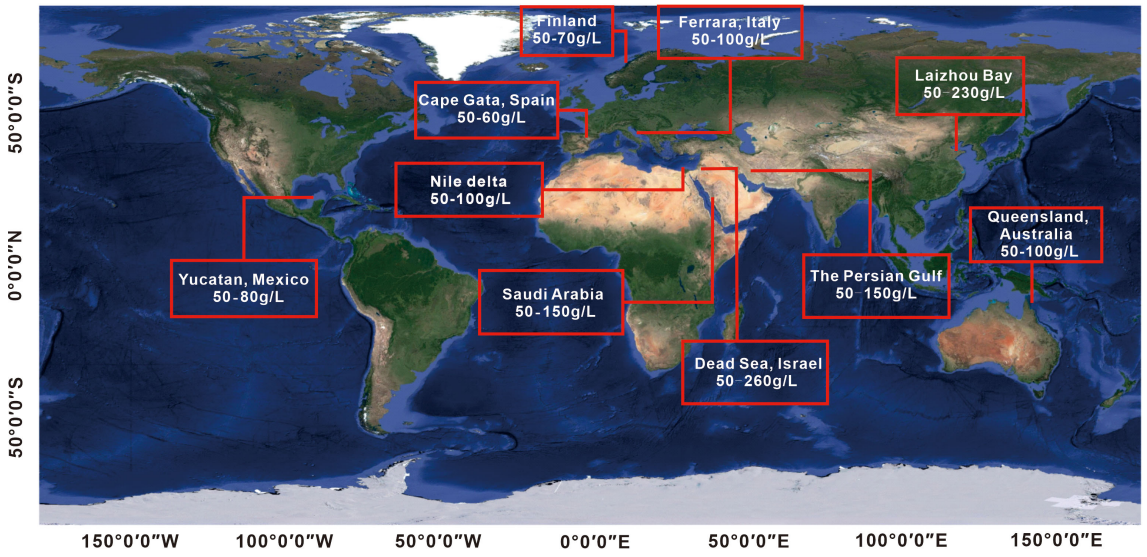

FIGURE 1
Global distribution of brine along coastlines.

Giambastiani et al., 2013; Aref & Taj, 2017; Saint-Loup et al., 2018; Van Engelen et al., 2018; Gil-Meseguer et al., 2019; Omerspahic et al., 2022; Jurikova et al., 2023).

2.1 Study area

The study area has a temperate continental to semi-arid climate, with average annual rainfall ranging from 500-600 mm and evaporation ranging from 1700-1900 mm. Rainfall is mainly concentrated in the July-August period. The topography of the study area is higher in the southern part and lower in the northern part, resulting in lower topography in the coastal area compared to the southern part of Laizhou Bay. The piedmont alluvial-proluvial and marine plains serve as the regional groundwater recharge and discharge zones, respectively. The central part of the piedmont alluvial-proluvial plain is the groundwater transition zone (Chen et al., 2004; Xu and Ding, 2008; Feng, 2016; Guo, 2016). The WF80 borehole is located in the groundwater discharge area, where the sources of groundwater recharge are complex. These sources include brine in the palaeosedimentary environment, lateral water flow from the Yu River, subsurface runoff from the southern region, atmospheric precipitation, and seawater from Laizhou Bay (Figure 2).

2.2 Background of groundwater salinization

The southern coastal area of Laizhou Bay is affected by changes in relative sea level, resulting in the development of marine and continental strata in alternating sequences. Previous studies have identified three high paleo sea-level periods in the southern coastal area of Laizhou Bay in the southern Bohai Sea since the late Pleistocene: Cangzhou (Qp_3^1), Xian (Qp_3^3), and Huanghua (Q_4) transgressions (Figure 2A). These transgressions have led to the formation of three sets of vertical marine strata, which have resulted in the presence of abundant underground brine mineral deposits in the southern coastal area of Laizhou Bay (Zhao et al., 1978; Han and Wu, 1982; Xu and Wang, 1990; Gao et al., 2015; Zhang et al., 1996; Wang et al., 2003; Yang, 2016; Yang et al., 2016).

Previous research has shown that the total dissolved solids (TDS) in the three marine brine strata exhibit a zonal distribution pattern from the southern (land area) to northern (sea area) parts of the study area (Zheng et al., 2014; Gao et al., 2015). The coastal area and the distant coastal area, spanning a width of 4-8 km and 5-10 km respectively, have low TDS contents (<100 g/L). In contrast, the central part of the south coast of Laizhou Bay displays high TDS contents (>100 g/L) over a width range of 10-15 km (Zhang and Peng, 1998; Leng et al., 2009; Gao et al., 2015; Yang, 2016). Specifically, the brine water within each marine stratum exhibits varying TDS contents: 50 to 140 g/L for the uppermost layer, 50 to 165 g/L for the intermediate layer, and 50 to 130 g/L for the lowermost layer (Figures 2B–D). Additionally, the saline aquifer in the southern coastal area extends seaward, resulting in higher TDS contents in the submarine groundwater compared to the surrounding seawater (Figure 2E) (Bi et al., 2012; Zheng et al., 2014; Gao et al., 2015; Liu, 2018).

2.3 Borehole description

The WF80 borehole (119.26741 E°; 37.20253 N°) is located in the Yu River Delta of the southern coastal area of Laizhou Bay (Figure 2A). The Lz908 borehole, on the other hand, is situated near the south coast of the Bohai Sea, China (118.97 E°; 37.15 N°) (Figure 2A). The Lz908 borehole was drilled to a depth of 101.3 m in the summer of 2007 by the First Institute of Oceanography, State

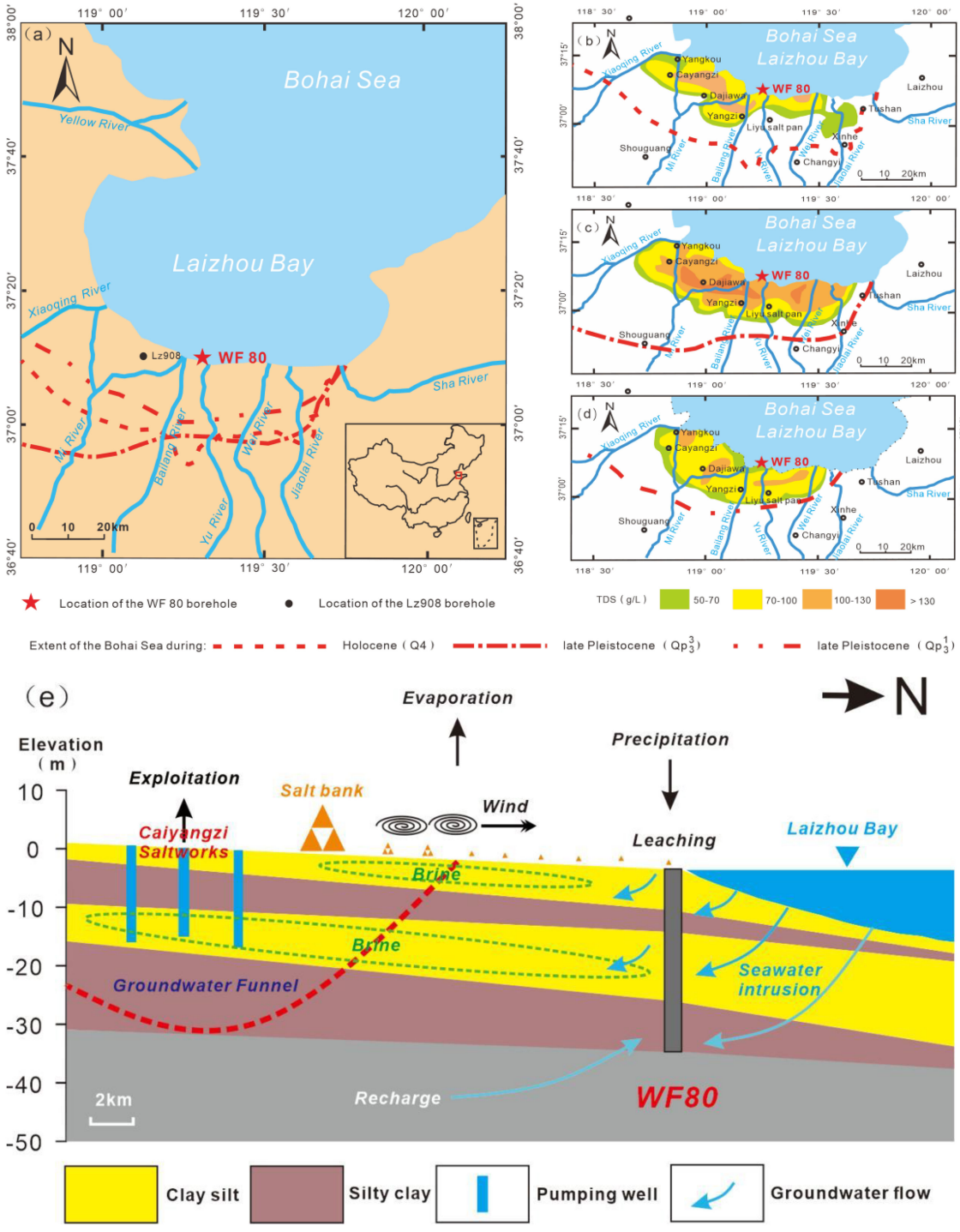

FIGURE 2
Location of WF80 and Lz908 boreholes in the study area. Seawater transgression extents during Late Pleistocene and Holocene **(A)**; Spatial distribution of TDS contents in brine water during Holocene (Q_4) **(B)**, Late Pleistocene (Qp_3^3) **(C)**, and Late Pleistocene (Qp_3^1) **(D)** [modified from Zheng et al., 2014], Geological section showing the distribution of groundwater quality and flow directions from hydrological data and the location of groundwater sampling site and monitoring wells. The hydrogeological profile is based on geological and hydrological data from past research and monitoring data (Modified from Han et al., 2014) **(E)**.

Oceanic Administration, China. The WF80 borehole is part of the delta cluster formed by the Weihe and Mihe rivers (Xue and Ding 2008) between the eastern and western branches of the Yishu Fault in the Shandong section of the Tancheng-Lujiang Fault Zone. In August 2020, core drilling was conducted in the WF80 borehole, with a core length of 78.2 m. For this study, the upper 36.6 m layer, which consists of fluvial and coastal sediments, was selected. Below 36.6 m, there is a dense semi-water-resisting layer with a thickness

of 5-6 m and significant lithologic changes. Prior to 2017, the WF80 drilling site was located in the intertidal zone with a seawater depth of approximately 1 m. However, land reclamation in 2017 raised the altitude to 4.3 m. The lithology of the upper 36.6 m layer, including 5.3 m of artificial backfill, primarily consists of yellow-gray clay, silty clay, clay silt, and silty sand. The North China Plain, including the study area, has experienced stable sedimentary conditions with consistent strata and no major unconformities or topographic reliefs (Wu et al., 2006). This provides a relatively complete record of environmental changes in both marine and terrestrial settings. Wang et al. (1981) reported that the southern coastal area of Laizhou Bay has undergone three cycles of seawater transgression and regression since the late Pleistocene. These cycles have led to the formation of various sediment facies, including neritic, delta, tidal flat, littoral neritic, and continental facies. During the seawater transgression period, littoral neritic sediment facies developed and retrograded to delta/tidal flat-fluvial sediments. The contribution of fluvial sediments from the Yu River decreased, while sediments from the Yellow River increased. Conversely, during the seawater regression period, there was an increase in terrigenous input, resulting in the development of fluvial facies and delta progradation (Gao et al., 2018).

2.4 Sediment and porewater sampling and analysis

In this study, we collected a total of 319 sediment samples from the study area to analyze their particle sizes. The samples were collected at intervals of 1-2 cm. We used a MASTERSIZER-2000 laser particle size meter to determine the sediment particle sizes (Appendix 1). To remove organic matter from the sediment samples, we first mixed them evenly and then mixed 1g of sediment with 10-15 ml of 30% hydrogen peroxide (H_2O_2) at room temperature. We added 5-10 ml of 10% hydrochloric acid (HCl) to remove calcium carbonate. The sediment samples were then mixed with distilled water and stored for 24 hours before being centrifuged. In addition, we collected 70 porewater samples from the WF80 borehole to analyze their hydrochemical characteristics. The porewater samples were collected at intervals of 50 cm. We used ion chromatography (ICS-3000, American DIONEX) to determine the concentrations of major anions (Cl^-, Br^-, and SO_4^{2-}) and inductively coupled plasma-atomic emission spectrometer (ICP-MS, American Thermo Fisher) to determine the concentrations of major cations (Ca^{2+}, Na^+, and Mg^{2+}) (Table 1). Before analyzing the cation concentrations, we acidified the collected porewater samples to a pH of approximately 2 using a nitric acid (HNO_3) solution. The charge balance errors of the porewater samples were less than 8%.

In this study, we used an LGR liquid water isotope laser mass spectrometry at Nanjing Hydraulic Research Institute to analyze the stable isotopic compositions (^{18}O and ^{2}H). The $\delta^{18}O$ and $\delta^{2}H$ values were calculated using Equations (1) and based on the Vienna Standard Mean Ocean Water (VSMOW). The analytical precision values for the long-term standard measurement of $\delta^{18}O$ and $\delta^{2}H$ were ±0.2‰ and ±0.6‰, respectively (Table 1).

$$\delta^{18}O(\delta^{2}H) = \frac{R_{Sample} - R_{VSMOW}}{R_{VSMOW}} \times 1000‰ \quad (1)$$

In formula (1), $\delta^{18}O$ and $\delta^{2}H$ represent the ratios of oxygen ($^{18}O/^{16}O$) and hydrogen ($^{2}H/^{1}H$) isotopes, respectively. R_{sample} represents the ratio of ^{18}O or ^{2}H in the porewater samples, while R_{VSMOW} represents the ratio of ^{18}O or ^{2}H in the VSMOW.

3 Results

3.1 Sedimentary characteristics and division of sedimentary units

In this study, we conducted sedimentary unit (SU) and sedimentary facies analyses of the Lz908 borehole using optically stimulated luminescence (OSL) and K-feldspar/polymineralplRIR$_{290}$ age (Unpublished data from Yan Li, China University of Geosciences) (Figure 3). The division of sedimentary units was based on the lithology, color, particle size, shell contents, porewater content, and other characteristics of the WF80 borehole sediment samples. The WF80 borehole can be classified into four SUs:

Sedimentary unit A (SUA) (5.3-12.8m): The OSL dating value at 12.8m from the bottom was 12.66 ± 1.05 ka B.P, indicating that Layer A is a marine sedimentary layer formed during the Holocene seawater transgression.

Sedimentary unit B (SUB) (12.8-16.45m): It is important to note that no pore water was observed in the SUB layer. The OSL dating value at 14.8m was older than 48.52 ka B.P, suggesting that SUB is a continental confining bed formed during the late Pleistocene.

Sedimentary unit C (SUC) (16.45-30.8m): In this layer, the average particle size showed significant variation below 27m, with a lack of sand particles. The K-feldspar dating value at 17.6m of the borehole was 91.5 ± 7.7 ka B.P. Additionally, there were three peaks of foraminifera counts in this layer. Based on the relationship between global sea-level changes and foraminifera counts (Figure 4), it can be concluded that SUC is a marine sedimentary layer formed during the late Pleistocene seawater transgression (Liang et al., 2012; Yi et al., 2012a).

Sedimentary unit D (SUD) (30.8-36.6m) had a wide range of particle sizes, but was notably lacking in sand particles. This suggests that SUD is a fluvial sedimentary layer that formed during the middle Pleistocene.

To summarize, the formation of SUA and SUC can be attributed to a period of high sea levels with abundant brine, while SUB and SUD were formed during a period of low sea levels.

3.2 Hydrochemical characteristics of the porewater

The porewater samples from SUA, SUC, and SUD showed different average ion concentrations but had similar orders (Figure 5). The main cation and anion concentrations followed the order of $Na^+ > Mg^{2+} > Ca^{2+}$ and $Cl^- > SO_4^{2-} > Br^-$, respectively. Na^+ and Cl^- accounted for more than 75% of the milligram

10.3389/fmars.2023.1302064

TABLE 1 Results of chemical analyses and stable isotopes of water samples.

Depth (m)	Cl- (mg/L)	Br- (mg/L)	SO_4^{2-} (mg/L)	Na^+ (mg/L)	Mg^{2+} (mg/L)	Ca^{2+} (mg/L)	δ D (‰)	$\delta^{18}O$ (‰)
5.5	15356.1	46.1	2327.6	6166.5	906.3	318.3	-21.0	-3.6
5.8	17588.6	51.1	2122.7	6877.5	1031.0	314.0	-19.4	-3.1
6.4	18186.4	52.4	2484.7	6778.5	1043.9	297.0	-19.6	-3.1
7.6	17174.7	50.5	2455.1	6738.0	1011.2	366.8	-17.1	-2.6
8.3	17232.0	48.0	2715.8	6388.5	966.2	369.8	-10.9	-2.0
8.7	17871.6	50.5	2218.8	6567.0	962.0	381.2	-13.3	-1.7
9.5	17020.7	43.8	2167.1	6093.0	881.6	349.4	-14.0	-1.8
9.8	17304.9	47.7	2225.7	6183.0	936.6	367.8	-15.6	-2.4
10.4	17366.8	48.6	2197.8	6388.5	921.3	365.0	-15.6	-2.9
10.7	17002.2	43.4	2180.7	6402.0	927.6	379.8	-13.7	-2.3
11.6	14556.3	40.7	1908.9	5590.5	760.8	317.7	-17.9	-2.7
12.4	14920.5	44.9	1942.2	6090.0	906.3	375.2	-12.8	-2.6
16.7	16020.6	46.9	2116.1	6138.0	837.8	431.4	-16.7	-2.2
17.8	15287.0	50.2	2095.3	6078.0	842.7	398.1	-18.0	-3.0
19.1	15582.8	50.8	2008.3	6139.5	853.8	393.0	-20.3	-3.5
19.8	14969.3	44.4	2935.7	6102.0	849.3	396.8	-17.0	-3.2
21.8	15373.1	46.8	1841.2	6078.0	855.3	374.6	-16.5	-2.7
22.1	16022.1	46.8	2097.2	5806.5	798.2	410.6	-16.1	-2.8
23.8	15433.6	48.2	2044.7	6381.0	903.8	420.6	-16.3	-2.5
24.5	15162.2	45.8	2033.9	6060.0	840.5	433.2	-17.7	-2.8
24.8	14318.5	46.4	1996.3	5985.0	831.0	423.3	-17.0	-2.8
28.3	15492.3	49.6	2137.4	5593.5	790.2	414.0	-10.3	-3.0
29.9	15242.8	48.9	2100.0	5992.5	847.5	433.5	-20.4	-3.3
30.1	16056.8	46.9	2903.8	5787.0	810.3	452.1	-19.0	-3.1
33.7	15164.0	45.6	2074.7	5805.0	805.5	400.1	-20.3	-3.1
34.3	15351.6	42.6	2110.3	5944.5	826.7	403.2	-19.7	-3.2
35.7	13242.5	40.5	1944.2	5574.0	734.4	377.1	-26.4	-4.0
36.3	12675.1	40.3	2121.1	5203.5	696.0	343.1	-27.2	-4.0
36.6	13641.0	40.6	2088.0	5218.5	714.9	345.8	-27.7	-4.3

equivalent percentages, while HCO_3^- concentrations were negligible. The hydrochemical characteristics of the porewater in SUA, SUC, and SUD were consistent with local seawater, indicating a Na-Cl facies type according to the Shukarev classification method.

These characteristics differed significantly from those observed in the southern brine water area with high total dissolved solids (TDS>50g/L)(Zhang, 1993; Zhang and Peng, 1998; Leng et al., 2009; Gao et al., 2015; Yang, 2016). However, the hydrochemical characteristics of the porewater in SUA, SUC, and SUD were relatively similar to those of the local coastal seawater. The porewater in SUA had higher average Na^+, Mg^{2+}, Cl^-, SO_4^{2-}, and Br^- concentrations compared to SUC and SUD, while the average Ca^{2+} concentration in SUA was lower. The concentrations of Na^+, Mg^2+, Cl^-, SO_4^{2-}, and Br^- in SUA showed significant changes with depth compared to SUC and SUD. These concentrations were generally higher than those in seawater, while Ca^{2+} concentrations were generally lower. The hydrochemical characteristics of the porewater in SUC showed slight changes and were relatively similar to seawater. In SUD, the concentrations of hydrochemical parameters gradually decreased

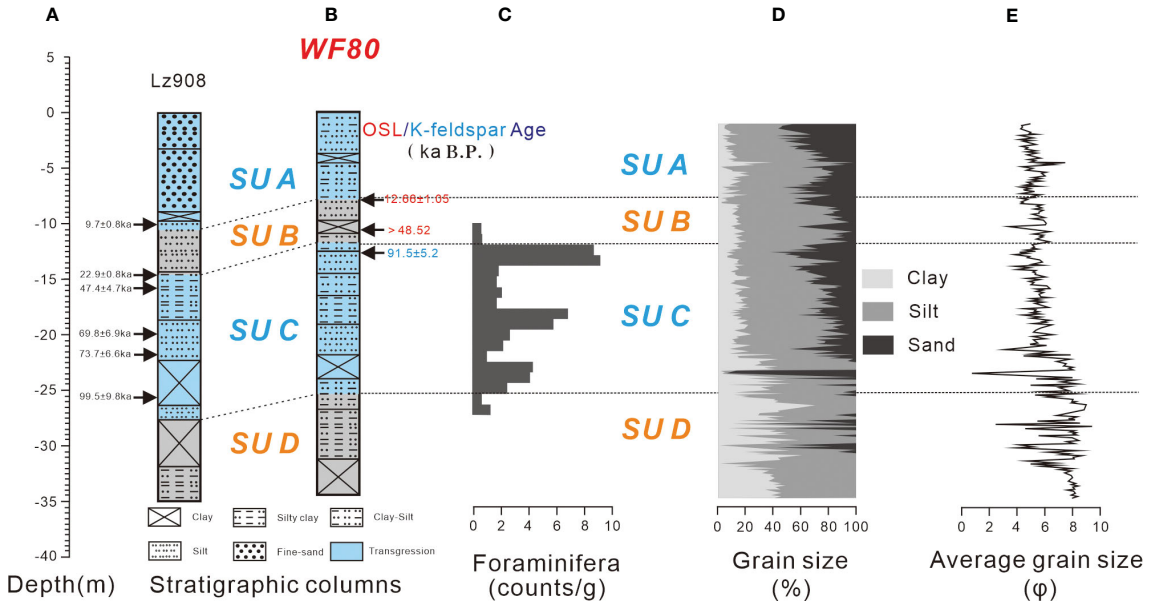

FIGURE 3
Stratigraphic columns and OSL age of Lz908 borehole **(A)**; Stratigraphic columns (excluding backfill soil) and OSL/K-feldspar ages of WF80 borehole **(B)**; Foraminiferal counts in WF80 borehole **(C)**; Sediment grain size in WF80 borehole **(D)**; Average grain sizes of sediments in WF80 borehole **(E)**.

with depth near the water-resisting layer. The porewater in SUA and SUC had similar characteristics to seawater due to the presence of a potential high-salinity brine layer. However, the water-resisting layer in the 12-16 m sediment layer caused slightly different ion distributions in the porewater of SUA and SUC. This could be attributed to the interaction between evaporation, seawater, and aerosol deposition in the southern salt-pan area. The concentrations of Na^+, Mg^{2+}, Cl^-, SO_4^{2-}, and Br^- in the porewater of SUA might increase near the surface due to rainwater infiltration and storm surges, while the Ca^{2+} concentration decreased due to the formation of gypsum through the bonding of Ca^{2+} and SO_4^{2-}. The concentrations of hydrochemical parameters in SUD were lower than those in SUA and SUC.

3.3 Isotopic characteristics of porewater

In this study, we analyzed the $\delta^{18}O$ and δD values of porewater samples to investigate the sources of porewater in the study area. The $\delta^{18}O$ and δD stable isotopes can be used to identify the sources and mixing history of water molecules in different waters, based on the global meteoric water line (GMWL) equation ($\delta D=8\delta^{18}O + 10$) (Chen et al., 2021). The local meteoric water line (LMWL) equation for Laizhou Bay was determined as $\delta D=7.4\delta^{18}O+1.1$, using the isotopic compositions of monthly precipitation recorded at the Changyi weather station in 2006. The average annual $\delta^{18}O$ and δD values of infiltrated rainwater in Laizhou Plain were -7.7 and -52.2‰, respectively. In the southern mountains of Shouguang, the

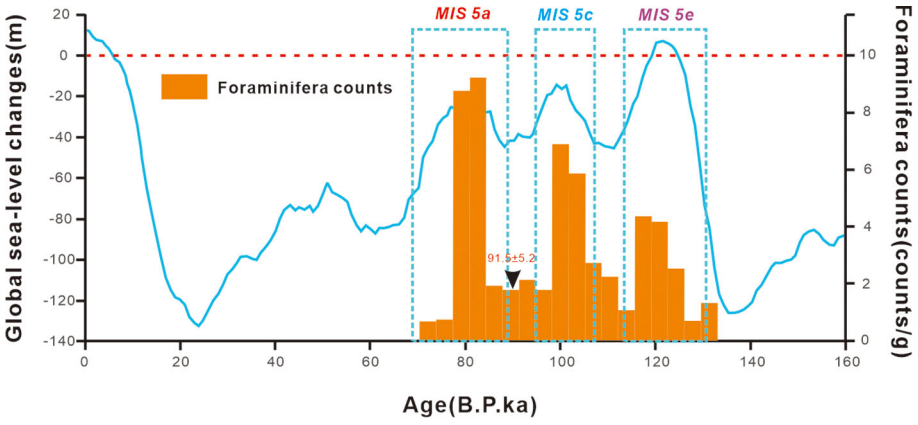

FIGURE 4
Foraminifera counts versus global sea level changes (Siddall et al., 2003). The blue dashed box corresponds to Marine Isotope Stage (MIS) 5 (A, C) and (E).

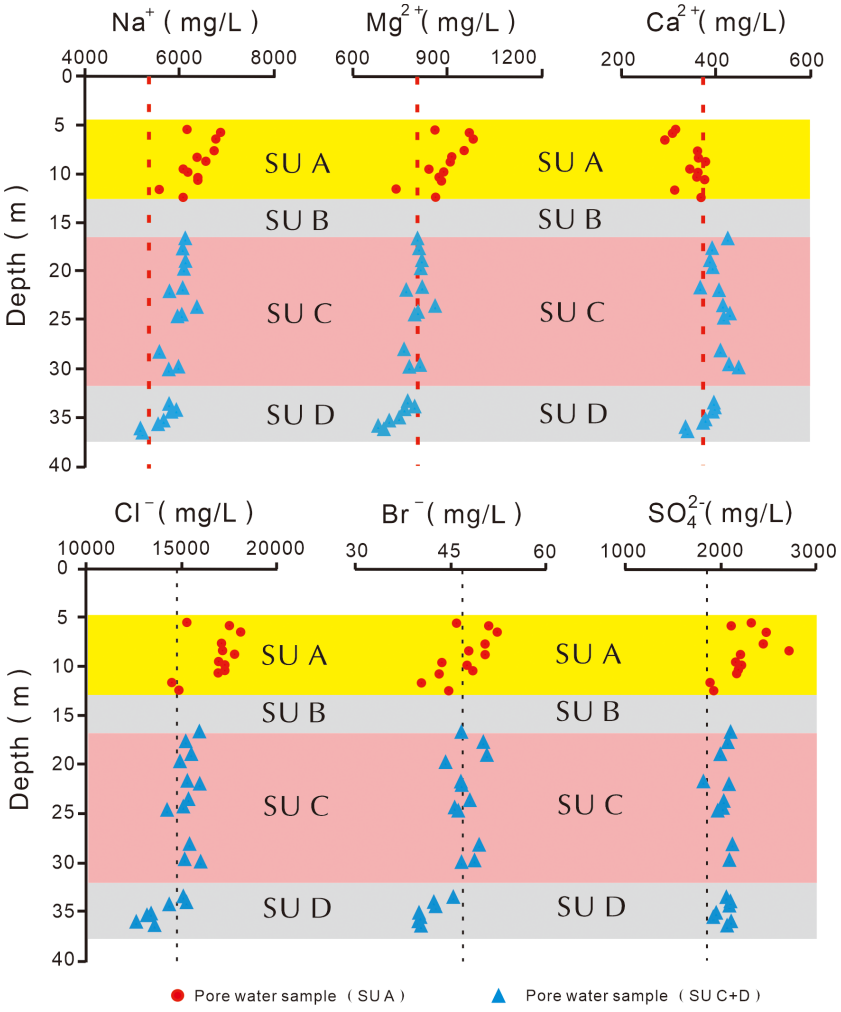

FIGURE 5
Vertical distributions of Na^+, Mg^{2+}, Ca^{2+}, Cl^-, Br^-, and SO_4^{2-} concentrations in porewater of WF80 borehole. Black dashed lines represent average concentration values of local seawater.

average annual $\delta^{18}O$ and δD values of infiltrated rainwater were -8.3 and -59.3‰, respectively (Yang et al., 2016).

Based on Figure 6, the δD and $\delta^{18}O$ values of SUA ranged from -21.0 to -10.9‰ and -3.6‰ to -1.7‰, respectively. The δD and $\delta^{18}O$ values of SUC ranged from -20.4 to -10.3‰ and -3.5 to -2.2‰, respectively. For the five continuous data points of SUD, the δD and $\delta^{18}O$ values ranged from -27.7 to -22.6‰ and -4.3 to -3.8‰, respectively. Most of the stable isotope values of porewater samples from SUA and SUC were plotted between the GMWL and LMWL, with only a few values plotted below the LMWL. The lines representing the δD and $\delta^{18}O$ values of SUA and SUC were similar and can be expressed by the equation: $\delta D = 5.2\delta^{18}O-3.5$. These lines intersect with the GMWL and LMWL, while the extension line passes through the stable isotope data points of local seawater.

4 Discussion

4.1 Groundwater dynamics

The ions profile (Figure 5) suggests that the sedimentation funnel caused by subsurface brine mining activities in the southern part of Laizhou Bay (Liu, 2018) may have influenced the groundwater dynamics. This resulted in a hydraulic gradient close to 0 in the horizontal direction on both sides of SUC, leading to a dynamic equilibrium with seawater. The horizontal direction of water flow is generally stable. However, brine mining reduced the porewater pressure in SUC, causing freshwater from the lower fluvial facies to flow through different sediment layers. This dilution process resulted in lower ion concentrations in the bottom SUD layers compared to the average ion concentrations of the SUC porewater.

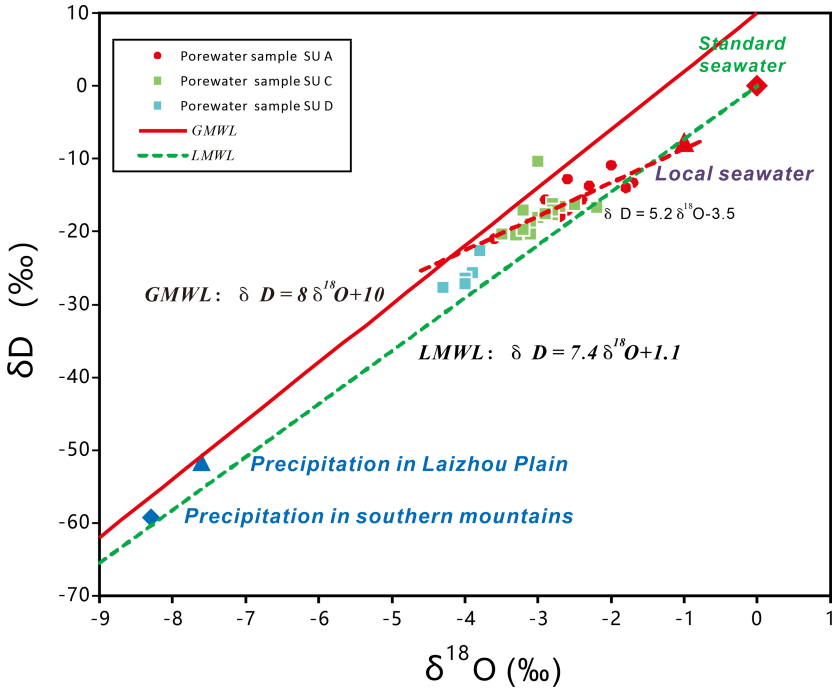

FIGURE 6
Relationships between δD and $\delta^{18}O$ values of porewater samples. Red dashed line represents fitted least squares regression of groundwater stable isotope values in study area ($\delta D = 5.2\delta^{18}O - 3.5$).

4.2 Salt sources in the porewater

Groundwater can acquire salt from various sources, including seawater intrusion, mobilization of salt from groundwater formation, and dissolution of evaporites in marine deposits (Zhou and Li, 1995; Han et al., 2011). The Cl/Br ratio can be used to identify the sources of groundwater salinity, especially when the total dissolved solids (TDS) content is high (above 2-3 g/L) (Cartwright et al., 2006; Du et al., 2015). In our study, the TDS content in the porewater samples from the WF80 borehole was significantly higher than 2-3 g/L, indicating the effectiveness of the Cl/Br method in determining the sources of porewater salinity.

The concentrations of Cl^- and Br^- in the world's oceans are relatively constant, with an average Cl/Br molar ratio of approximately 655 (Cl^- = 550 mmol/L and Br^- = 0.84 mmol/L) (Siemann, 2003). However, the concentrations of Cl^- and Br^- can vary in marginal seas due to factors such as terrigenous inputs and brine chemical wastewater discharge. In our study, the Cl/Br molar ratio of the local seawater was approximately 710 (Cl^- = 417.18 mmol/L and Br^- = 0.59 mmol/L), which is higher than the average value of the ocean.

The Cl/Br ratio values of the porewater samples from SUA, SUC, and SUD were similar to that of the local seawater and lower than those found in dissolved evaporated salt and diluted brine (Figure 7). Notably, there were significant differences between the variations in Cl/Br ratio and Cl^- concentrations in SUA and SUC. The Cl/Br ratios in SUA ranged from 748.8 to 883.2, with an average of 801.3, which was higher than that of the local seawater. These data points were mainly associated with high Cl^- concentrations. The average Cl/Br ratios in SUC and SUD were lower than that of SUA, ranging from 686.8 to 771.7 and 708.7 to 812.4, respectively. However, it is important to mention that six points in SUC had lower Cl/Br ratios than the average Cl/Br ratio of the local seawater, indicating lower Cl concentrations ranging from 14318.5-15582.8 mg/L.

The observed Cl/Br ratios suggest that marine salt is the primary source of salinity in the porewaters of SUA, SUC, and SUD. High Cl/Br ratios may be attributed to halite dissolution, while low values may indicate brine dilution. However, it is challenging to determine whether the porewater was diluted by seawater. Overall, SUA exhibited high Cl^- concentrations and Cl/Br ratio values, with substantial variations in Cl^- concentrations at different depths. This suggests that the porewater in SUA is influenced by evaporation, precipitation, dissolution, and infiltration processes of salts in the southern salt pans. These salts may be transported from the southern salt pans by the south wind. On the other hand, the observed Cl/Br ratio values in SUC were lower than the average seawater value, indicating the presence of small amounts of brine in this layer.

4.3 Porewater sources

The δD and $\delta^{18}O$ values of SUA and SUC were significantly different from the average annual stable isotope values of rainwater in the Laizhou Plain and southern mountain areas (Figure 6). SUC data points were concentrated between the Global Meteoric Water Line (GMWL) and Local Meteoric Water Line (LMWL), while the five data points of SUD were notably different from those of SUC, with negative δD and $\delta^{18}O$ values. These observations suggest that the porewaters of

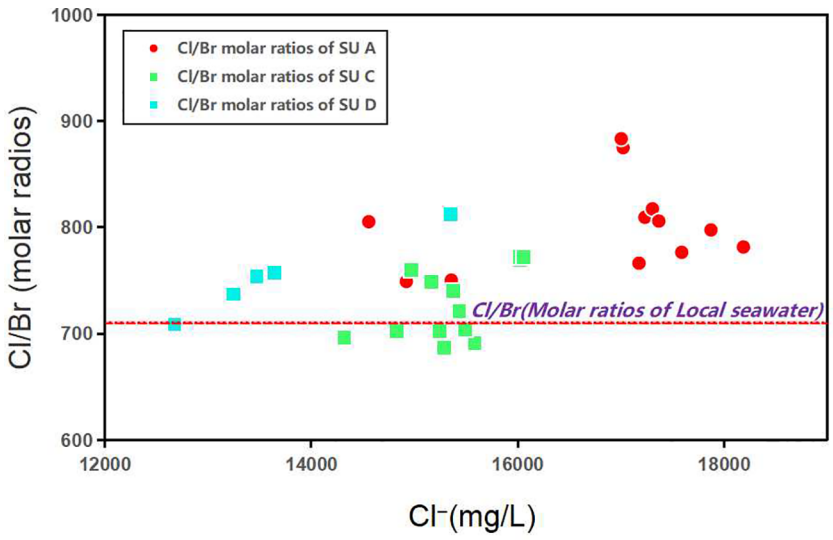

FIGURE 7
Relationship between Cl/Br ratio values (molar ratios) and Cl^- concentrations in porewater.

SUA and SUC mainly originated from local seawater, showing a slight correlation with the rainwater in the Laizhou Plain and southern mountain areas. Compared to SUC, the porewater samples from SUA had δD and $\delta^{18}O$ values closer to local seawater. Additionally, SUC exhibited greater stability and lower water exchange capacity, as indicated by the more concentrated δD and $\delta^{18}O$ values in Figure 6. The porewater samples of SUD were more influenced by the water-bearing layers below the water-resisting layers, and they were mixed with water characterized by ion concentrations much lower than that of seawater in the water-bearing layers below the water-resisting layers (Figures 5, 6).

In summary, as mentioned in Sections 4.2 and 4.3, marine salt was identified as the primary source of salt in the porewater of the WF80 borehole. The porewater mainly originated from local seawater, as indicated by the relatively consistent Na^+, Mg^{2+}, Ca^{2+}, Cl^-, SO_4^{2-}, and Br^- concentrations with those in local seawater. Therefore, the saline water occupying the original brine layer is likely derived from seawater through modern seawater intrusion.

4.4 Porewater mixing in groundwater salinization process

The stable properties of $\delta^{18}O$ and Cl^- have been studied by Kelln et al. (2001) and Nefzaoui et al. (2023). The $\delta^{18}O$ values of groundwater are closely related to the mixing of water sources. Therefore, the deviation of observed $\delta^{18}O$ and Cl^- values from the mixing lines can be used to identify the main sources of water mixing (Chen et al., 2021). In the Yu River delta, there are four water resources that affect groundwater: seawater, rainwater, Yu River water, and brine. This study investigates the relationship between $\delta^{18}O$ values and Cl^- concentrations to assess porewater mixing in the WF80 borehole (Figure 8).

The results show that the $\delta^{18}O$ values of SUA, SUC, and SUD increase with increasing Cl^- concentrations in the porewater. These values fall between the mixing line of local seawater with rainwater and that of brine with rainwater. The observed values are closer to the mixing line of seawater with rainwater. The data points are classified into three regions. The data points of SUA are close to the values of local seawater, exhibiting high $\delta^{18}O$ values and Cl^- concentrations. The data points of SUC are plotted in the middle, parallel to the data points of SUA, with lower $\delta^{18}O$ values and Cl^- concentrations. The data points of SUD are located in the lower part, deviating from seawater values, and exhibiting the lowest $\delta^{18}O$ values and Cl^- concentrations. These findings support the previous results, suggesting that SUA and SUC represent brine layers, while SUD experienced infiltration of upper brine. Although the brine was displaced by seawater, a small amount of residual brine mixed with the intruded seawater. The porewaters of SUA and SUC have the same source, with SUA being more affected by salt dissolution and infiltration from salt pans carried by the south wind. In contrast, the porewater of SUC is relatively stable, while that of SUD is more influenced by water inputs from the lower layer, characterized by low salinity.

5 Conclusions

The study shows that fluctuations in paleo sea levels are crucial in determining the distribution of underground water sources in coastal areas. Groundwater exploitation and seawater intrusion have a significant impact on the process of groundwater salinization at different depths in regions with original brine layers. The depth at which salt is leached from atmospheric precipitation is limited. The extraction of groundwater and the intrusion of seawater have greatly altered the original state of

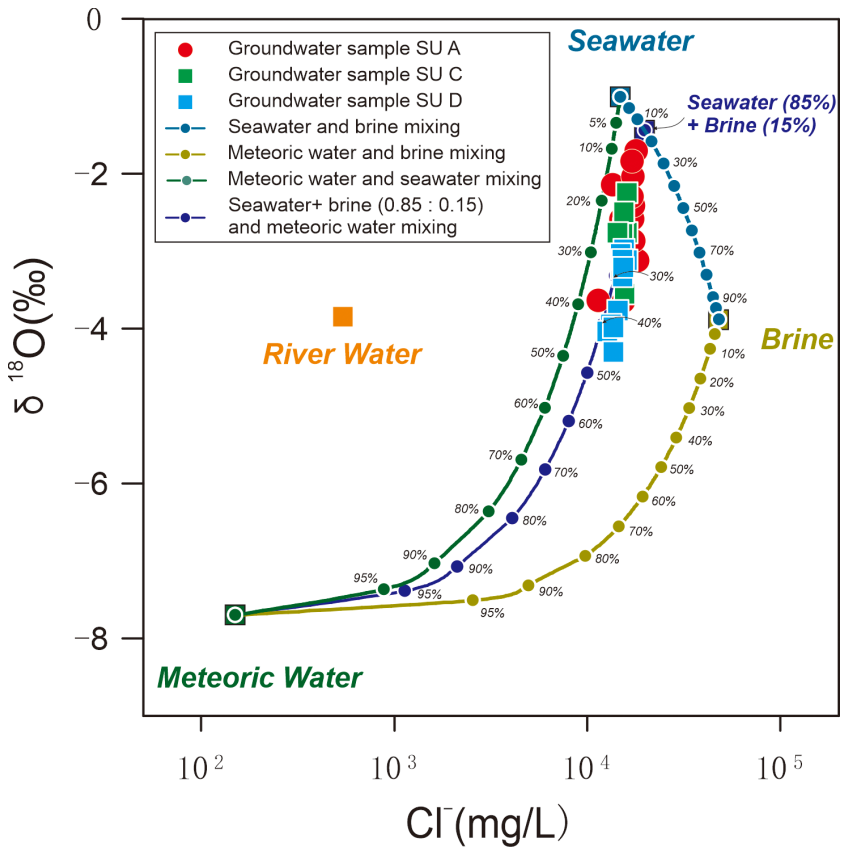

FIGURE 8
Relationship between observed $\delta^{18}O$ values and Cl^- concentrations in porewater samples. Average $\delta^{18}O$ value and Cl^- concentration in local seawater were -1.0‰ and 14809.8 mg/L, respectively. Annual average $\delta^{18}O$ value and Cl^- concentration in rainwater were -7.7‰ and 115 mg/L, respectively. Average $\delta^{18}O$ value and Cl^- concentration in Yu River water were -2.93‰ and 697 mg/L, respectively. Average $\delta^{18}O$ value and Cl^- concentration in brine of study area were -3.88‰ and 48054 mg/L, respectively.

the groundwater. Most of the brine layer has been replaced by modern seawater, but a small portion remains mixed with seawater. Groundwater extraction changes the flow of groundwater and reduces the pressure of water in the underground sources. The intrusion of seawater and the recharge of other stratified water bodies have caused fundamental changes in the chemical and isotopic properties of the groundwater. This mechanism of salinization may also be applicable to similar areas worldwide.

Data availability statement

The raw data supporting the conclusions of this article will be made available by the authors, without undue reservation.

Author contributions

ZC: Writing – original draft, Writing – review & editing, Conceptualization, Data curation, Formal Analysis. GC: Conceptualization, Funding acquisition, Writing – review & editing. SC: Conceptualization, Supervision, Writing – review & editing. HY: Conceptualization, Writing – review & editing. KC: Conceptualization, Formal Analysis, Writing – review & editing. BR: Software, Writing – review & editing. TF: Formal Analysis, Writing – review & editing. WL: Resources, Writing – review & editing. YW: Resources, Writing – review & editing. XJ: Writing – review & editing. XZ: Writing – review & editing.

Funding

The author(s) declare financial support was received for the research, authorship, and/or publication of this article. We thank the basic data provided by Observation and Research Station of Seawater Intrusion and Soil Salinization through the First Institute of Oceanography (FIO) Ministry of Natural Resources (MNR). This research was supported by The Joint Funds of the National Natural Science Foundation of China under contract No.U22A20580; U2106203; National Natural Science Foundation of China under contract No.42276223; 41706067; 41876077; Open Project Program of Key Laboratory of Ecological Warning, Protection & Restoration for Bohai Sea, Ministry of Natural Resources (2022108).

Acknowledgments

We thank the basic data provided by Observation and Research Station of Seawater Intrusion and Soil Salinization through the First Institute of Oceanography (FIO) Ministry of Natural Resources (MNR).This research was supported by The Joint Funds of the National Natural Science Foundation of China under contract No.U22A20580; U2106203; National Natural Science Foundation of China under contract No.42276223; 41706067; 41876077; Open Project Program of Key Laboratory of Ecological Warning, Protection & Restoration for Bohai Sea, Ministry of Natural Resources (2022108).

Conflict of interest

The authors declare that the research was conducted in the absence of any commercial or financial relationships that could be construed as a potential conflict of interest.

Publisher's note

Supplementary material

The Supplementary Material for this article can be found online at: https://www.frontiersin.org/articles/10.3389/fmars.2023.1302064/full#supplementary-material

APPENDIX 1
Granular data.

References

Acworth, R. I., and Dasey, G. R. (2003). Mapping of the hyporheic zone around a tidal creek using a combination of borehole logging, borehole electrical tomography and cross-creek electrical imaging, New South Wales, Australia. *Hydrogeology J.* 11 (3), 368–377. doi: 10.1007/s10040-003-0258-4

Agossou, A., Yang, J., and Lee, J. (2022). Evaluation of potential seawater intrusion in the coastal aquifers system of Benin and effect of countermeasures considering future sea level rise. *Water* 14 (24), 4001. doi: 10.3390/w14244001

Alcalá, F. J., and Custodio, E. (2008). Using the Cl/Br ratio as a tracer to identify the origin of salinity in aquifers in Spain and Portugal. *J. Hydrology* 359 (1-2), 189–207. doi: 10.1016/j.jhydrol.2008.06.028

Alessandrino, L., Gaiolini, M., Cellone, F. A., Colombani, N., Mastrocicco, M., Cosma, M., et al. (2023). Salinity origin in the coastal aquifer of the Southern Venice lowland. *Sci. Total Environ.* 905, 167058. doi: 10.1016/j.scitotenv.2023.167058

Aref, M. A., and Taj, R. J. (2017). Hydrochemical characteristics of sabkha brines, evaporite crystallization and microbial activity in Al-Kharrar sabkha and their implication on future infrastructures in Rabigh area, Red Sea coastal plain of Saudi Arabia. *Environ. Earth Sci.* 76 (10), 1–18. doi: 10.1007/s12665-017-6686-6

Balasubramanian, M., Sridhar, S. G. D., Ayyamperumal, R., Karuppannan, S., Gopalakrishnan, G., Chakraborty, M., et al. (2022). Isotopic signatures, hydrochemical and multivariate statistical analysis of seawater intrusion in the coastal aquifers of Chennai and Tiruvallur District, Tamil Nadu, India. *Mar. pollut. Bull.* 174, 113232. doi: 10.1016/j.marpolbul.2021.113232

Bi, Y., Yu, H., Xu, X., and Su, Q. (2012). Chemical characteristics of groundwater in the southern plain of Laizhou Bay. *Mar. Bull.* 03), 241–247.

Bordbar, M., Busico, G., Sirna, M., Tedesco, D., and Mastrocicco, M. (2023). A multi-step approach to evaluate the sustainable use of groundwater resources for human consumption and agriculture. *J. Environ. Manage.* 347, 119041. doi: 10.1016/j.jenvman.2023.119041

Carretero, S., Rodrigues Capítulo, L., Dapeña, C., Fabiano, M., and Kruse, E. (2022). A chemical and isotopic approach to investigate groundwater dynamics in a coastal aquifer. *Catena* 213, 106229. doi: 10.1016/j.catena.2022.106229

Cartwright, I., Weaver, T. R., and Fifield, L. K. (2006). Cl/Br ratios and environmental isotopes as indicators of recharge variability and groundwater flow: An example from the southeast Murray Basin, Australia. *Chem. Geology* 231 (1-2), 38–56. doi: 10.1016/j.chemgeo.2005.12.009

Cartwright, I., Weaver, T. R., Fulton, S., Nichol, C., Reid, M., and Cheng, X. (2004). Hydrogeochemical and isotopic constraints on the origins of dryland salinity, Murray Basin, Victoria, Australia. *Appl. Geochemistry* 19 (8), 1233–1254. doi: 10.1016/j.apgeochem.2003.12.006

Chappell, J., Omura, A., Esat, T., McCulloch, M., Pandolfi, J., Ota, Y., et al. (1996). Reconciliaion of late Quaternary sea levels derived from coral terraces at Huon Peninsula with deep sea oxygen isotope records. *Earth Planetary Sci. Lett.* 141 (1), 227–236. doi: 10.1016/0012-821X(96)00062-3

Chen, G., Guiyao, X. J. L. X., Hongjun, Y., Wenquan Liu, T. F. Q. S., and Xilai Zheng, A. C. P. (2021). Research article elucidating the pollution sources and groundwater evolution in typical seawater intrusion areas using hydrochemical and environmental stable isotope technique: A case study for Shandong province, China. *GeoScienceWorld* 18, 4227303. doi: 10.2113/2021/4227303/5398230/4227303

Chen, J., Tang, C., Sakura, Y., Kondoh, A., Yu, J., Shimada, J., et al. (2004). Spatial geochemical and isotopic characteristics associated with groundwater flow in the North China Plain. *Hydrological Processes* 18 (16), 3133–3146. doi: 10.1002/hyp.5753

Du, Y., Ma, T., Chen, L., Shan, H., Xiao, C., Lu, Y., et al. (2015). Genesis of salinized groundwater in Quaternary aquifer system of coastal plain, Laizhou Bay, China: Geochemical evidences, especially from bromine stable isotope. *Appl. Geochemistry* 59, 155–165. doi: 10.1016/j.apgeochem.2015.04.017

Dun, Y., Ling, J., Wang, R., Wei, J., Zhou, Q., Cao, Y., et al. (2022). Hydrochemical evolution and nitrogen behaviors in coastal groundwater suffered from seawater intrusion and anthropogenic inputs. *Front. Mar. Sci.* 9. doi: 10.3389/fmars.2022.945330

Edmunds, W. M., Ma, J., Aeschbach-Hertig, W., Kipfer, R., and Darbyshire, D. P. F. (2006). Groundwater recharge history and hydrogeochemical evolution in the Minqin Basin, North West China. *Appl. Geochemistry* 21 (12), 2148–2170. doi: 10.1016/j.apgeochem.2006.07.016

Feng, S. (2016). *Laizhou bay water chemical characteristics and submarine groundwater discharge* (Beijing: China university of geosciences). a master's degree thesis.

Gao, M., Guo, F., Hou, G., Qiu, J., Kong, X., and Liu, S. (2018). Sedimentary evolution of Laizhou Bay, Southern Bohai Sea since Late Pleistocene. *China Geology* 01), 59–68.

Gao, M., Zheng, Y., Liu, S., Wang, S., Kong, X., Zhao, J., et al. (2015). Paleogeographic conditions analysis of laizhou bay underground brine formed. *Geological Rev.* 02), 393–400.

Giambastiani, B. M. S., Colombani, N., Mastrocicco, M., and Fidelibus, M. D. (2013). Characterization of the lowland coastal aquifer of Comacchio (Ferrara, Italy): Hydrology, hydrochemistry and evolution of the system. *J. Hydrology* 501, 35–44. doi: 10.1016/j.jhydrol.2013.07.037

Gil-Meseguer, E., Gómez-Espín, J. M., and Bernabe-Crespo, M. B. (2019). Desalination and water security in Southeastern Spain. *J. Political Ecol.* 26 (1), 486–499. doi: 10.2458/v26i1.22911

Guo, F. (2016). *The sedimentary evolution of laizhou bay since late pleistocene and provenance analysis* (east China: a master's degree thesis, China university of petroleum).

Guo, Z., and Huang, Y. (2003). A review of research on seawater intrusion. *Hydrology* 03, 10–15.

Han, D., Cao, G., Currell, M. J., Priestley, S. C., and Love, A. J. (2020). Groundwater salinization and flushing during glacial-interglacial cycles: insights from aquitard porewater tracer profiles in the north China plain. *Water Resour. Res.* 56 (11). doi: 10.1029/2020WR027879

Han, D., Kohfahl, C., Song, X., Xiao, G., and Yang, J. (2011). Geochemical and isotopic evidence for palaeo-seawater intrusion into the south coast aquifer of Laizhou Bay, China. *Appl. Geochemistry* 26 (5), 863–883. doi: 10.1016/j.apgeochem.2011.02.007

Han, D. M., Song, X. F., Currell, M. J., Yang, J. L., and Xiao, G. Q. (2014). Chemical and isotopic constraints on evolution of groundwater salinization in the coastal plain

aquifer of Laizhou Bay. *China. J. hydrology (Amsterdam)* 508, 12–27. doi: 10.1016/j.jhydrol.2013.10.040

Han, Y., and Wu, H. (1982). The origin of underground brine in the coastal plain of Laizhou Bay. *Geological Rev.* 28 (2), 126–131. doi: 10.3321/j.issn:0371-5736.1982.02.005

Hendry, M. J., and Woodbury, A. D. (2007). Clay aquitards as archives of holocene paleoclimate: δ18O and thermal profiling. *Groundwater* 45 (6), 683–691. doi: 10.1111/j.1745-6584.2007.00354.x

Jurikova, H., Ring, S. J., Henehan, M. J., Neugebauer, I., Schröder, B., Müller, D., et al. (2023). Boron geochemistry reveals the evolution of Dead Sea brines. *Earth Planetary Sci. Lett.* 622, 118403. doi: 10.1016/j.epsl.2023.118403

Kelln, C. J., Wassenaar, L. I., and Hendry, M. J. (2001). Stable isotopes (δ18O, δ2H) of pore waters in clay-rich aquitards: A comparison and evaluation of measurement techniques. *Groundwater Monit. Remediation* 21 (2), 108–116. doi: 10.1111/j.1745-6592.2001.tb00306.x

Laattoe, T., Werner, A. D., and Simmons, C. T. (2013). *Seawater Intrusion Under Current Sea-Level Rise: Processes Accompanying Coastline Transgression* (Springer Netherlands), 295–313.

Larsen, F., Tran, L. V., Van Hoang, H., Tran, L. T., Christiansen, A. V., and Pham, N. Q. (2017). Groundwater salinity influenced by Holocene seawater trapped in incised valleys in the Red River delta plain. *Nat. Geosci.* 10 (5), 376–381. doi: 10.1038/ngeo2938

Lenahan, M. J., and Bristow, K. L. (2010). Understanding sub-surface solute distributions and salinization mechanisms in a tropical coastal floodplain groundwater system. *J. Hydrology* 390 (3), 131–142. doi: 10.1016/j.jhydrol.2010.06.009

Leng, Y., Li, X., and Liu, L. (2009). Characteristics and genesis of the natural brine deposit in the north of Weifang, Shandong, China. *J. Chengdu Univ. Technol. (Natural Sci. Edition)* 36 (2), 188–194.

Liang, Y., Hong-Jun, Y., Joseph, D. O., Xing-Yong, X., Shen-Liang, C., Jun-Yi, G., et al. (2012). Late Quaternary linkage of sedimentary records to three astronomical rhythms and the Asian monsoon, inferred from a coastal borehole in the south Bohai Sea, China. *Palaeoecology*, 329–330.

Lio, C. D., Carol, E., Kruse, E., Teatini, P., and Tosi, L. (2015). Saltwater contamination in the managed low-lying farmland of the Venice coast, Italy: An assessment of vulnerability. *Sci. Total Environ.* 533, 356–369. doi: 10.1016/j.scitotenv.2015.07.013

Liu, S. (2018). *Evolution of laizhou bay underground salt water and salt water intrusion process mechanism research* (China university of geosciences). Ph.D. Dissertation.

Liu, S., Tang, Z., Gao, M., and Hou, G. (2017). Evolutionary process of saline-water intrusion in Holocene and Late Pleistocene groundwater in southern Laizhou Bay. *Sci. Total Environ.* 607-608, 586–599. doi: 10.1016/j.scitotenv.2017.06.262

Moussaoui, I., Rosa, E., Cloutier, V., Neculita, C. M., and Dassi, L. (2023). Chemical and isotopic evaluation of groundwater salinization processes in the Djebeniana coastal aquifer, Tunisia. *Appl. Geochemistry* 149, 105555. doi: 10.1016/j.apgeochem.2022.105555

Nefzaoui, F., Ben Hamouda, M. F., Carreira, P. M., Marques, J. M., and Eggenkamp, H. G. M. (2023). Evidence for groundwater salinity origin based on hydrogeochemical and isotopic (2H, 18O, 37Cl, 3H, 13C, 14C) approaches: sousse, eastern Tunisia. *Water* 15 (6), 1242. doi: 10.3390/w15061242

Omerspahic, M., Al-Jabri, H., Siddiqui, S. A., and Saadaoui, I. (2022). Characteristics of desalination brine and its impacts on marine chemistry and health, with emphasis on the persian/arabian gulf: A review. *Front. Mar. Sci.* 9. doi: 10.3389/fmars.2022.845113

Parisi, A., Alfio, M. R., Balacco, G., Güler, C., and Fidelibus, M. D. (2023). Analyzing spatial and temporal evolution of groundwater salinization through Multivariate Statistical Analysis and Hydrogeochemical Facies Evolution-Diagram. *Sci. Total Environ.* 862, 160697. doi: 10.1016/j.scitotenv.2022.160697

Petelet-Giraud, E., Négrel, P., Aunay, B., Ladouche, B., Bailly-Comte, V., Guerrot, C., et al. (2016). Coastal groundwater salinization: Focus on the vertical variability in a multi-layered aquifer through a multi-isotope fingerprinting (Roussillon Basin, France). *Sci. Total Environ.* 566-567, 398–415. doi: 10.1016/j.scitotenv.2016.05.016

Rajmohan, N., Masoud, M. H. Z., and Niyazi, B. A. M. (2021). Impact of evaporation on groundwater salinity in the arid coastal aquifer, Western Saudi Arabia. *Catena* 196, 104864. doi: 10.1016/j.catena.2020.104864

Saint-Loup, R., Felix, T., Maqueda, A., Schiller, A., and Renard, P. (2018). A survey of groundwater quality in Tulum region, Yucatan Peninsula, Mexico. *Environ. Earth Sci.* 77 (18), 1–20. doi: 10.1007/s12665-018-7747-1

Sanford, W. E., Doughten, M. W., Coplen, T. B., Hunt, A. G., and Bullen, T. D. (2013). Evidence for high salinity of Early Cretaceous sea water from the Chesapeake Bay crater. *Nature* 503 (7475), 252–256. doi: 10.1038/nature12714

Sathish, S., Chanu, S., Sadath, R., and Elango, L. (2022). Impacts of regional climate model projected rainfall, sea level rise, and urbanization on a coastal aquifer. *Environ. Sci. pollut. Res.* 29 (22), 33305–33322. doi: 10.1007/s11356-021-18213-8

Siddall, M., Rohling, E. J., Almogi-Labin, A., Hemleben, C., Meischner, D., Schmelzer, I., et al. (2003). Sea-level fluctuations during the last glacial cycle. *Nat. (London)* 423 (6942), 853–858.

Siemann, M. G. (2003). Extensive and rapid changes in seawater chemistry during the Phanerozoic: evidence from Br contents in basal halite. *Terra Nova* 15 (4), 243–248. doi: 10.1046/j.1365-3121.2003.00490.x

Tomaszkiewicz, M., Abou Najm, M., and El-Fadel, M. (2014). Development of a groundwater quality index for seawater intrusion in coastal aquifers. *Environ. Model. Software* 57, 13–26. doi: 10.1016/j.envsoft.2014.03.010

Vallejos, A., Sola, F., Yechieli, Y., and Pulido-Bosch, A. (2018). Influence of the paleogeographic evolution on the groundwater salinity in a coastal aquifer. Cabo de Gata aquifer, SE Spain. *J. Hydrology* 557, 55–66. doi: 10.1016/j.jhydrol.2017.12.027

Van Engelen, J., Oude Essink, G. H. P., Kooi, H., and Bierkens, M. F. P. (2018). On the origins of hypersaline groundwater in the Nile Delta aquifer. *J. Hydrology* 560, 301–317. doi: 10.1016/j.jhydrol.2018.03.029

Wang, Z., Meng, G., and Wang, S. (2003). Geochemistry modeling of Quaternary subsurface brine in the south coast of Laizhou Bay, the Bohai Sea-taking brines from core- Aoli 501 in Changyi Area as an example. *Mar. geology Quaternary geology* 23 (1), 49–53. doi: 10.16562/j.cnki.0256-1492.2003.01.008

Wang, P., Min, Q., Bian, Y., and Cheng, X. (1981). Strata of Quaternary transgressions in East China: A preliminary study. *Acta Geologica Sin.* 1, 1–13. doi: 10.19762 / j.carol carroll nki dizhixuebao. 1981.01.001

Werner, A. D., Bakker, M., Post, V. E. A., Vandenbohede, A., Lu, C., Ataie-Ashtiani, B., et al. (2013). Seawater intrusion processes, investigation and management: Recent advances and future challenges. *Adv. Water Resour.* 51, 3–26. doi: 10.1016/j.advwatres.2012.03.004

Wu, S., Yu, Z., Zhou, D., and Zhang, H. (2006). Structural features and Cenozoic evolution of Tan-lu fault zone in the Laizhou Bay, Bohai Sea. *Mar. geology Quaternary geology* 26 (6), 101–110.

Xu, C., and Ding, D. (2008). Wei he River - Mi he River Delta in South Coast of Bohai Sea, China:Sedimentary Sequence and Archi tecture. *Scientia Geographica Sin.* 05, 672–676.

Xue, C., and Ding, D. (2008). Weizhe-mihe delta on the south bank of Laizhou Bay, Bohai Sea: sedimentary sequence and framework. *Scientia Geographica Sinica* (05), 672–676.

Xu, h., and Wang, S. (1990). Research progress of Quaternary coastal facies underground brine in China. *Adv. Earth Sci.* 04), 58–59.

Xu, Y., Wu, J., Xie, C., and Zhang, Y. (1997). Study on seawater intrusion and saltwater intrusion in coastal of Laizhou Bay. *Chin. Sci. Bull.* 22, 2360–2368.

Yakirevich, A., Melloul, A., Sorek, S., Shaath, S., and Borisov, V. (1998). Simulation of seawater intrusion into the Khan Yunis area of the Gaza Strip coastal aquifer. *Hydrogeology J.* 6 (4), 549–559. doi: 10.1007/s100400050175

Yang, Q. (2016). *Origin of Shallow Salt (Brine) Water Salinity in the Coast of Laizhou Bay* (China university of geosciences). Ph.D. Dissertation. Available at: https://kns.cnki.net/KCMS/detail/detail.aspxdbname=CDFDLAST2017&filename=1017126067.nh.

Yang, Q., Wang, R., Xu, S., Li, W., Wang, Z., Mei, J., et al. (2016). Hydrogeochemical and stable isotopic characteristics of brine in laizhou bay. *Geological Rev.* 62 (2), 343–352.

Yi, L., Yu, H., Ortiz, J. D., Xu, X., Qiang, X., Huang, H., et al. (2012a). A reconstruction of late Pleistocene relative sea level in the south Bohai Sea, China, based on sediment grain-size analysis. *Sedimentary Geology* 281, 88–100. doi: 10.1016/j.sedgeo.2012.08.007

Zhang, C. (1993). Origin and evolution of underground brine in coastal plain of Laizhou Bay. *J. Institute Hydrogeology Eng. Geology Chin. Acad. Geological Sci.* 9, 78–96.

Zhang, Z., and Peng, L. (1998). The underground water hydrochemical characteristics on sea water intruded in eastern and southern coasts of Laizhou. *China Environ. Sci.* 02, 26–30.

Zhang, Y., Xue, Y., and Chen, H. (1996). Characteristics of sedimentary seawater and formation environment in the late Pleistocene strata on the south coastal of Laizhou Bay. *Acta Oceanologica Sin.* 6), 61–68.

Zhao, S., Yang, G., Cang, S., Zhang, H., Huang, Q., Xia, D., et al. (1978). On the marine stratigraphy and coastlines of the western coast of the gulf of Bohai. *Oceanologia Et Limnologia Sin.* 01), 15–25.

Zheng, Y., Gao, M., Liu, S., Wang, S., Zhao, J., and Wang, C. (2014). Distribution characteristics of subsurface brine resources on the soutern coast of laizhou bay since late peistocene. *Hydrogeology Eng. Geology* 41 (5), 11–18.

Zhou, X., and Li, C. (1995). Seawater evaporation trajectories and their application. *Earth Sci.* 04), 410–414.